Discover Applied Sciences

Research

Microbial methanogenesis fueled by freshwater infiltration and oil biodegradation in the Siljan impact structure, Sweden

Femke van Dam[1] · Riikka Kietäväinen[2,7] · George Westmeijer[3,8] · Manuel Reinhardt[4] · Shuhei Ono[5] · Mark Dopson[3] · Marcelo Ketzer[1] · Jennifer C. McIntosh[6] · Henrik Drake[1]

Received: 8 May 2024 / Accepted: 6 December 2024
Published online: 03 January 2025

Abstract
Deeply fractured rocks of meteorite impact craters are suggested as prime niches for subsurface microbial colonization. Methane can be a product of such microbial communities and seeps of methane from impact craters on Earth are of strong interest as they act as analogs for Mars. Previous studies report signs of ancient microbial methanogenesis in the Devonian Siljan meteorite impact structure in Sweden, but the proportion of microbial methane, metabolic pathways, and potential modern activity remain elusive. In this study, gas composition, hydrochemistry, oil organic geochemistry, and microbial community analyses are reported in 400 m deep fractures of the Siljan impact structure. The results showed a dominantly microbial origin for methane, which was supported by highly negative $\delta^{13}C_{CH4}$ and positive $\delta^{13}C_{CO2}$ values along with multiply substituted isotopologues ($\Delta^{13}CH_3D$) that indicated disequilibrium fractionation due to microbial kinetic isotope effects. The presence of C_2 to C_5 hydrocarbons suggested a minor thermogenic input in the gas mix. Characterization of the microbial community via 16S rRNA gene amplicon sequencing and real-time PCR indicated a low abundance of several methanogenic archaeal populations, which is common for settings with active methanogenesis. Evidence of oil biodegradation suggested that secondary microbial hydrocarbon utilization was involved in the methanogenesis. Low sulfate and high alkalinity in the groundwaters also suggested a dominantly microbial methane formation driven by infiltration of freshwater that was coupled to sulfate reduction and secondary utilization of early mature thermogenic hydrocarbons.

Article highlights

1. Characterization of deep methane accumulations in a Siljan impact structure fracture aquifer.
2. Mixed microbial-thermogenic origin with microbial methanogenesis relating to inflow of freshwater and biodegradation.
3. 16S rRNA gene sequencing and real-time PCR suggest methanogens present in low abundance.

Supplementary Information The online version contains supplementary material available at https://doi.org/10.1007/s42452-024-06418-8.

✉ Femke van Dam, femke.vandam@lnu.se | [1]Department of Biology and Environmental Science, Linnaeus University, Kalmar, Sweden. [2]Geological Survey of Finland (GTK), Espoo, Finland. [3]Centre for Ecology and Evolution in Microbial Model Systems (EEMiS), Linnaeus University, Kalmar, Sweden. [4]Department of Geobiology, Univeristy of Göttingen, Göttingen, Germany. [5]Department of Earth, Atmospheric and Planetary Sciences, Massachusetts Institute of Technology, Cambridge, MA, USA. [6]Department of Hydrology and Atmospheric Sciences, University of Arizona, Tucson, USA. [7]Department of Geosciences and Geography, University of Helsinki, Helsinki, Finland. [8]Department of Chemistry, Umeå University, Umeå, Sweden.

Keywords Methanogens · Impact crater · Clumped isotopologues · Hydrocarbon degradation

1 Introduction

Meteorite impact craters may play an important role in creating and facilitating colonization of deep subsurface habitats on Earth, and potentially other planets and moons [1]. The environmental conditions generated by such impacts are favorable for microbial communities owing to bedrock fracturing during the impact and creation of pore space as well as enhancing hydrothermal circulation that can provide the energy required for maintaining underground life [2, 3]. Studying these systems on Earth can give a critical understanding of the methane cycles on Mars, where methane has been detected in the Gale crater [4, 5], as well as clarify how the high porosity and fracturing of impact crater systems may accumulate gas.

The Siljan impact crater (380.9 ± 4.6 Ma, [6]) is the largest in Europe and located in central Sweden (Fig. 1). The impact crater rim consists of 200 m to 600 m downfaulted and fractured sedimentary rocks of Ordovician and Silurian age, consisting of shales and limestones, which overlay Precambrian crystalline granitoid rocks [7]. Seepage of methane and oil has occurred in this impact crater for hundreds of years [8], but the origin of hydrocarbons is yet to be fully understood. Earlier studies propose the seeping methane to be of abiotic origin [9] and of thermogenic and/or microbial origin in more recent studies [10]. Reports of ancient biosignatures in rock fractures and hydrothermal systems in the impact crater include Hode et al. [11] who reported findings of putative extracellular polymeric substances of microorganisms, of unknown age, in fractured granite within the central uplift. In addition, Siljeström et al. [12, 13] reported on the presence of biomarkers in crude oils from the Siljan impact structure and in single oil-bearing fluid inclusions of calcite-fluorite veins in Ordovician rock of the impact structure. The organic-rich shales present in the Siljan impact structure are proposed to be the source rock for the oil and bitumen found in the area [14, 15]. In addition, the occurrence of microbial oil biodegradation has been proposed based on an investigation of seep oil and bitumen [14]. More recently, Drake et al. [10] found evidence of microbial methanogenesis in the rock record up to 80 million years ago, in the fractured aquifer of the impact structure based on stable carbon and sulfur isotopic signatures. Finally, Drake et al. [16] reported fossilized, chitin-bearing fungal hyphae at 537 m depth in granite underneath the sedimentary successions in the crater rim. Observations of fossilized anaerobic fungi preserved in fractures in the impact crater further suggests that the H_2 necessary for autotrophic methanogenesis could have been provided by fungi. There are thus several indications of paleomicrobiological activity in the impact crater. In contrast, there have been very few reports of the origin of the gas accumulations in the Siljan impact crater.

The microbial formation of CH_4 most commonly occurs under anoxic conditions at redox levels Eh < −200 mV [17] and is conducted by archaea of Euryarchaeota lineages. These methanogens can produce CH_4 through three main metabolic pathways: in the CO_2-reduction pathway H_2 is oxidized, and CO_2 is reduced to methane (hydrogenotrophic), organic carbon molecules like formate, methanol, methylamines (methylotrophic) can be utilized and/or by the acetoclastic pathway, where acetate is cleaved with the methyl group and reduced to CH_4. In the continental deep subsurface, the clades Methanobacteriales and Methanosarcinales are most common, but overall distribution is site-specific [18–20].

Although the microbiota of many impact craters hosted lakes have been examined, such as the Lonar [21] and Clearwater [22] impact lakes, the microbiota of the bedrock of the impact crater itself is seldom reported. One such study by Cockell et al. [23] reports microbiological enumerations in the Chesapeake Bay impact structure showing a relation between lithology and microbial abundance. Similarly, Cockell et al. [24] show taxonomically distinct microbial communities in each crater lithology based on the 16S rRNA gene of the Chicxulub crater. In other settings such as sedimentary basins, microbial methane generation can be stimulated by the inflow of meteoric water, by for instance lowering the sulfate concentrations [25–27]. That microbial methanogenesis might be linked to inflow of meteoric water has also been observed in fractured craton sites in e.g., South Africa [28]. However, lack of hydrogeochemical and microbiological data at the Siljan crater has so far hindered holistic models of the origin of methane here.

This study presents the results of a comprehensive sampling campaign and analyses of Siljan structure groundwater chemistry, isotopic composition of gases, and microbial communities from 400 m depth as well as organic geochemistry of the oil. Emerging methods such as clumped isotopes of methane may provide additional evidence for the origin of natural gas but has yet to be applied at Siljan. By providing new microbiological and geochemical evidence, the aim was to fill knowledge gaps in fundamental understanding of processes related to hydrocarbon generation in the Siljan structure with implications for other impact structures on Earth.

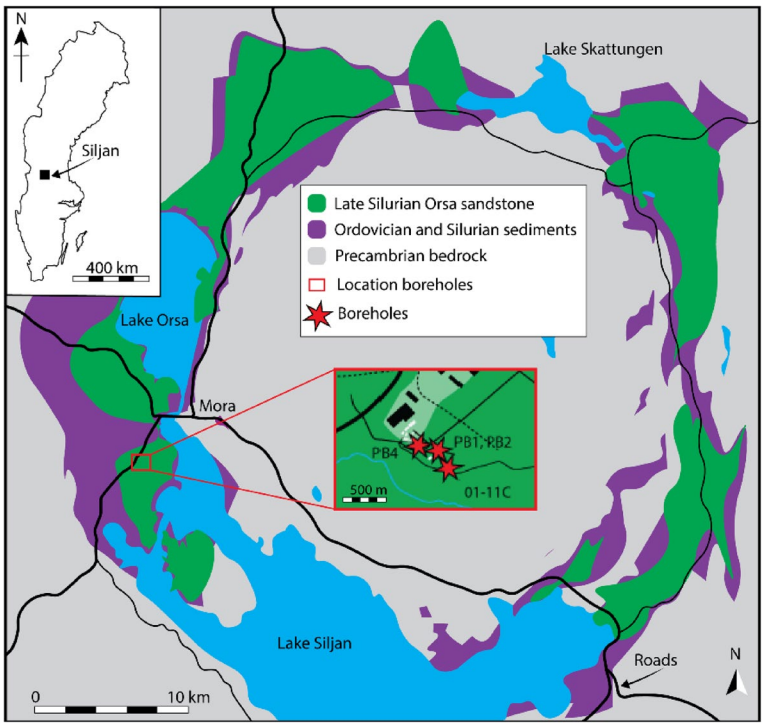

Fig. 1 Map of crater and field site with the location of boreholes. Borehole stratigraphy of PB2 is in supplementary Fig. 1. Modified after [7]

2 Materials and methods

2.1 Sampling and analyses

Field samples were taken in September 2021 from four boreholes in the Mora area, central Sweden, in the western part of the impact structure where sedimentary rocks crop out (Fig. 1). The samples consisted of free gas, groundwater, oil, and microbial biomass collected on filters.

Free gas samples were taken from three boreholes (named PB1, PB2, and PB4) using Isotubes (Isotech) connected to valves on the surface directly above the boreholes, as well as in Schott bottles using the water displacement methodology. The gas in the Schott bottles was analyzed by Applied Petroleum Technology, Oslo (APT) for chemical and isotope compositions. Hydrocarbons were identified and quantified with a gas chromatograph (GC) equipped with a flame ionization detector (FID), and H_2, CO_2, N_2, and O_2+Ar with a thermal conductivity detector (TCD). The GC for hydrocarbon analysis was an Agilent 7890 A instrument. The chromatographic column was a HP PONA (50 m length, 0.2 mm internal diameter, 0.5 µm film thickness). The temperature program of the GC-oven started at 30 °C (held for 10 min), followed by heating to 60 °C (held for 10 min) with 2 °C/min, heating to 130 °C with 2 °C/min, and heating to 320 °C (held for 25 min) with 4 °C/min. 2,2,4-tri-methyl-pentane was used as internal standard.

The stable carbon isotopic composition of the hydrocarbon components in the gas was determined by a gas chromatograph coupled to a combustion and isotope ratio mass spectrometer (GC-C-IRMS), with a reproducibility of $\delta^{13}C$ values better than 1‰ V-PDB (2 sigma). The methane hydrogen isotope composition was determined with a reproducibility of δD values better than 10‰ V-SMOW (2 sigma). The clumped isotopologues of methane in the free gas were measured at the Massachusetts Institute of Technology. For methane isotopologue analysis, methane was extracted and purified from gas samples following the preparative GC method described by Wang et al. [29]. The relative abundances of methane isotopologues $^{12}CH_4$, $^{13}CH_4$, $^{12}CH_3D$, and $^{13}CH_3D$ were measured using a tunable infrared laser direct absorption spectroscopy (TILDAS) described previously [30]. Values of $\delta^{13}C$ and δD of methane analyzed via TILDAS were calibrated via measurements of natural gas standards NGS-1 and NGS-3 [29]. The abundance of $^{13}CH_3D$ isotopologue was reported as $\Delta^{13}CH_3D$, a metric representing the deviation of the abundance of $^{13}CH_3D$ from a stochastic distribution of isotopes among isotopologues $^{12}CH_4$, $^{13}CH_4$, $^{12}CH_3D$, and $^{13}CH_3D$:

$$\Delta^{13}CH_3D = \frac{\left[^{13}CH_3D\right]\left[^{12}CH_4\right]}{\left[^{13}CH_4\right]\left[^{12}CH_3D\right]} - 1$$

The stochastic isotopologue ratios (i.e., $\Delta^{13}CH_3D = 0$) were determined by thermally equilibrating methane at 250 °C using Pt catalyst [30] and the theoretical fractionation factors of [31].

Groundwater samples for hydrochemistry and microbiology were pumped from ~ 380 m (slit at ~ 380 m) in borehole PB2. Prior to sampling, three borehole volumes were pumped and allowed to refill with its own groundwater to avoid contamination from stagnant water. Groundwater samples for hydrogeochemical analysis were taken as follows: 250 mL unfiltered samples were collected for anions and alkalinity, 100 mL filtered (pore size 0.45 µm) and acidified (500 µL of 65% ultrapure HNO_3) sample for cations, and 60 mL filtered (pore size 0.45 µm) sample for water stable isotopes ($\delta^{18}O_{H2O}$ and δD_{H2O}). DNA samples were collected under in situ pressure using an aluminum filter holder with a downstream valve (Millipore; as previously described in [32]) on filter membranes in triplicates by filtering (pore size 0.1 µm) 7.0 (filter #1), 11.2 (#2), and 10.9 L (#3) of groundwater. Flow rates during sampling through the filters were 95–158 mL min^{-1}. The filters were aseptically transferred to a collection tube and stored at −80 °C during transport from the field to the laboratory. Hydrogeochemical analysis was performed on the PB2 groundwater, which was analyzed for chemical composition (anions and cations) at Eurofins Environment Testing, Finland using ion chromatography, ICP-OES, and ICP-MS methods following standard protocols. Alkalinity was determined on site by titrating with 1.6 N sulfuric acid to pH 4.5 using a digital titrator (Hach). Water stable isotope analysis was carried out at the Geological Survey of Finland, Espoo using Picarro cavity ring-down spectrometer (CRDS).

A nearby borehole to the gas wells (01-11C) contained supernatant oil in the water column. The oil, which had seeped into the borehole from rock fractures along the borehole, was sampled and analyzed for organic geochemistry components at APT. Molecular composition of the oil was determined on an Agilent 7890 A GC instrument with a HP PONA column (length 50 m, i.d. 0.2 mm, film thickness 0.5 µm) with the same temperature program as described above. 2-heptene was used as an internal standard.

2.2 DNA extraction and amplification

DNA was extracted using the DNeasy PowerWater kit (Qiagen), following the manufacturer's protocol except for eluting the nucleic acids in 50 µL. The V3-V4 region of the 16S rRNA gene was amplified using the primer pair 341F and 805R [33]. The product of the first PCR served as a template for the second PCR containing the unique sequencing sequences. In total, the two amplification steps contained 32 cycles. The product was purified after each PCR step using the AMPure SP reagent (Beckman Coulter). The concentration of the amplified products was measured using a Qubit 2.0 fluorometer (Life Technologies) and the fragment length distribution was assessed using automated gel electrophoresis. Sequencing of the PCR product library was performed at the Science for Life Laboratory, Sweden on an Illumina MiSeq platform, producing 2 × 301 bp paired-end reads [32].

The archaeal abundance was estimated by quantifying the 16S rRNA gene copies using real-time PCR (qPCR) on a LightCycler 480 (Roche Diagnostics). The reaction volume (10 µL) consisted of 5 µL Platinum SYBR Green qPCR SuperMix-UDG with ROX (Thermo Fisher Scientific), 0.4 µL 10 µM primer, 3.2 µL nuclease-free water, and 1.0 µL template. Archaeal gene fragments were amplified using the primers 915F and 1059R [34]. Cycling conditions were 2 min at 95 °C, 40 cycles of 15 s at 95 °C and 30 s at 60 °C, followed by a melt curve analysis to assess product specificity. Standard curves were generated with a dilution series of purified PCR product using genomic DNA extracted from a *Ferroplasma acidiphilum* BRGM4 pure culture as template. Standards ($n = 7$), test samples, and no-template controls were run in triplicates and the former two were 1:10 diluted in nuclease-free water to account for inhibition of the polymerase. The results were reported in gene copies mL^{-1} after correcting for the volume of groundwater used for DNA extraction and the elution volume. A minimum and maximum reaction efficiency of 85 and 115% was maintained, respectively. A minimum number of three quantification cycles (ΔCq) between samples and no-template controls were maintained as a limit of detection.

2.3 16S rRNA sequence analysis

Raw sequences from the 16S rRNA gene amplicon (V3-V4 region) were processed using the ampliseq v2.3.0 pipeline [35] from the nf-core framework [36]that used Nextflow (v21.10.6), Cutadapt (v3.4), FastQC (v0.11.9), DADA2 (v1.22.0), and the SBDI Sativa curated 16S rRNA gene GTDB database (release 207, [37]). The ampliseq pipeline was run with default

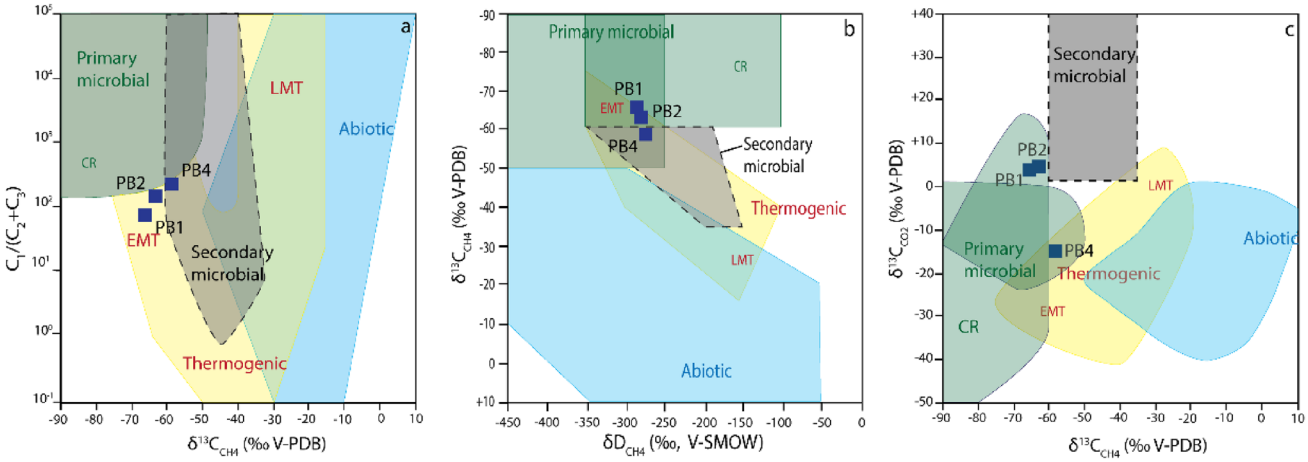

Fig. 2 Gas origin discrimination diagrams. a. $C_1/(C_2+C_3)$ vs $\delta^{13}C_{CH4}$; b. $\delta^{13}C_{CH4}$ vs δD_{CH4} c. $\delta^{13}C_{CO2}$ vs $\delta^{13}C_{CH4}$. Figure after [39]

Table 1 Isotope values of boreholes PB1, 2, 4 and oil-associated gas (APT data), in permille V-PDB

	$\delta^{13}C_{C1}$	$\delta^{13}C_{C2}$	$\delta^{13}C_{C3}$	$\delta^{13}C_{i\text{-}C4}$	$\delta^{13}C_{n\text{-}C4}$	$\delta^{13}C_{CO2}$	δD_{C1}
PB1	−65.8	−31.7	−17.7	−28.6	−27.4	5.5	−284
PB2	−63.2	−30.2	−14.5	−27.9	–	6.4	−279
PB4	−58.8	−29.8	−14.9	−28.2	–	−13.8	−273
Oil	−56.8	−35.3	−28.6	−28.9	−27.7	–	–

parameters, except for the trimming of the primers whereby reads not containing the primer sequence or containing double copies were discarded from downstream analyses [38].

3 Results

3.1 Gas compositions, isotopes, and isotopologues

3.1.1 Compositions

The gas composition in the three boreholes (PB1, PB2 and PB4, supplementary Table 1) was dominated by methane (94–99 vol.% of total hydrocarbon gas) with small quantities of ethane (1.2–0.4%) and propane (< 0.1%). The ratios of methane to heavier chain hydrocarbons, i.e., $C_1/(C_2+C_3)$, ranged from 73 to 218 (Fig. 2a). Carbon dioxide was present in PB1 at 5%, PB2 at 2.4%, and PB4 at 0.02%. Helium concentration was < 0.04%, H_2 was below detection limit (< 10 ppm), while N_2 was 0.84, 0.66, 38.3%, and O_2 + Ar was 0.27, 0.32 and 9.54% for PB1, PB2, and PB4, respectively.

3.1.2 Stable isotopes

Methane had $\delta^{13}C$ values of −65.8, −63.2, and −58.8‰ V-PDB for boreholes PB1, PB2, and PB4, respectively (Fig. 2a, Table 1). The PB1 and PB2 $\delta^{13}C_{CH4}$ values were also measured during the isotopologue measurement for different Isotube subsamples from the same sampling campaign (Table 2), for which the results were similar to the measurements specifically executed for stable carbon isotopes (−65.7 and −63.4‰ V-PDB for PB1 and PB2, respectively). The carbon stable isotopes and the $C_1/(C_2+C_3)$ ratios suggested a mixed origin, from which the proportion of microbial methane vs. an early mature thermogenic origin can be estimated. The latter was more prominent for the methane in well PB1, whereas microbial methane was more prominent in well PB4 (Fig. 2a). The early mature thermogenic origin of methane was less clear when comparing δD and $\delta^{13}C$ of CH_4 values, as these samples also plotted within the primary microbial field (Fig. 2b). The carbon isotope composition of CO_2 ($\delta^{13}C_{CO2}$) ranged from −13.8‰ for PB4 to + 5.5 and + 6.4‰ for PB1 and PB2, respectively that plotted in $\delta^{13}C_{CH4}$ plots within the carbonate reduction microbial field, quite close to secondary

Table 2 Methane clumped isotopologues and apparent equilibration temperatures for PB1 and PB2, in duplicate

	$\delta^{13}C_{C1}$	δD_{C1}	$\Delta^{13}CH_3D$	Temp (°C)	+	–
PB1a	−65.75 ± 0.06	−271.7 ± 0.26	3.5 ± 0.31	121.75	19.77	17.65
PB1b	−65.77 ± 0.06	−271.71 ± 0.06	3.6 ± 0.17	116.43	10.2	9.603
PB2a	−63.39 ± 0.07	−266.02 ± 0.06	4.1 ± 0.15	86.75	7.43	7.15
PB2b	−63.46 ± 0.04	−266.02 ± 0.06	4.1 ± 0.31	88.69	15.95	14.49

Hydrogen isotopes of methane measured by APT had values of −284‰ in PB1 and −279‰ in PB2; the corresponding values from MIT show a systematic difference of 13‰ V-SMOW

microbial for PB1 and PB2 (Fig. 2c). However, caution needs to be taken when interpreting the PB4 $\delta^{13}C_{CO2}$ results, as the CO_2 concentration was low and there was possible air contamination, as indicated by the $Ar + O_2$ and N_2 values.

Ethane had $\delta^{13}C$ values of −31.7, −30.2, and −29.8‰ for PB1, PB2 and PB4, respectively that suggested a thermogenic origin, occurring together with methane of dominantly microbial origin (Fig. 3). Propane had a $\delta^{13}C$ values of −17.7, −14.5, and −14.9‰ for PB1, PB2, and PB4, respectively. In PB1, both iso-butane and n-butane were present and had $\delta^{13}C$ values of −28.6 and −27.4‰, respectively. In PB2 and PB4 only iso-butane was detected ($\delta^{13}C$ values: −27.9 and −28.2%, respectively).

3.1.3 Isotopologues

Methane clumped isotopologues, $\Delta^{13}CH_3D$ values, of samples from boreholes PB1 and PB2 were measured in duplicate for each sub-sample giving 3.5 ± 0.2 and 3.6 ± 0.3‰ for PB1 and 4.1 ± 0.2‰ and 4.1 ± 0.3‰ for PB2. These values corresponded to apparent methane formation temperatures of 121 ± 19.8 °C and 116 ± 10.2 °C for PB1 and lower temperatures for PB2 of 87 ± 7.4 °C and 89 ± 16 °C, respectively.

When $\Delta^{13}CH_3D$ was plotted vs $\delta^{13}C_{CH4}$ (Fig. 4), the PB1 and PB2 samples were in a field where microbial methane has been reported previously [29, 41, 42], and close to studies reporting a mixture of microbial and thermogenic methane [41, 43].

3.2 Oil organic geochemistry and gas component

The whole oil chromatogram was dominated by *n*-alkanes (*n*-C_3 to *n*-C_{33}) (Fig. 5). The *n*-alkane abundance increased strongly at *n*-C_{12}, and a maximum was visible at *n*-C_{13}. Bulk parameters of the oil also reflected the strong aliphatic character, including 68.1 wt% saturates, 23.1 wt% aromatics, 8.4 wt% polar compounds, and 0.4 wt% asphaltenes. An unresolved complex mixture (UCM) hump was present in the area of higher molecular weight *n*-alkanes (Fig. 5). The *n*-C_7/$MCyC_6$ ratio was 0.20, the Tol/*n*-C_7 ratio was 0.34, the Pr/*n*-C_{17} ratio was 0.56, and the Ph/*n*-C_{18} ratio was 0.29 (Table 3). Tr1 to Tr7 ranged between 0 and 2.94 (Table 3). The carbon isotopic ratios of the different oil fractions were −30.7‰ for the saturates and −30‰ for the aromatics.

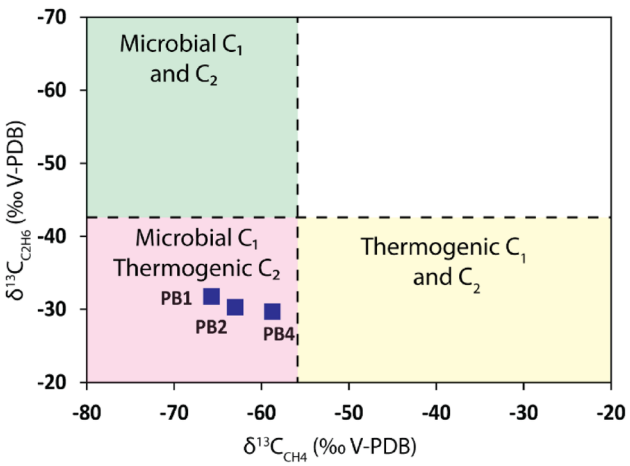

Fig. 3 $\delta^{13}C$ of ethane (C_2) versus methane (C_1), after Taylor et al. [40]

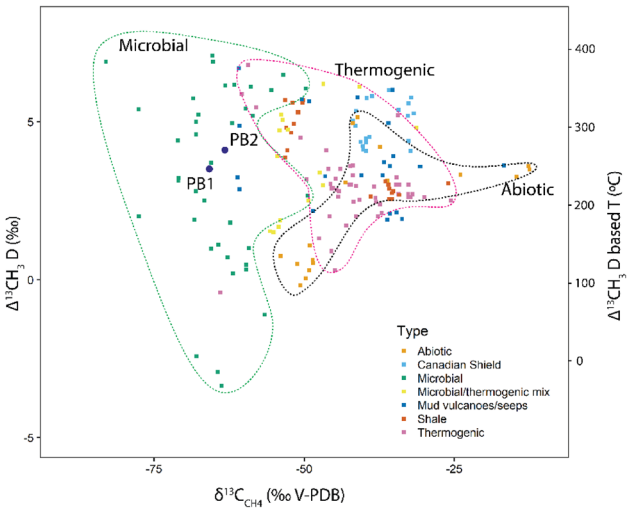

Fig. 4 $\Delta^{13}CH_3D$ vs $\delta^{13}C_{CH4}$ values against previously published background data [29, 41–48]

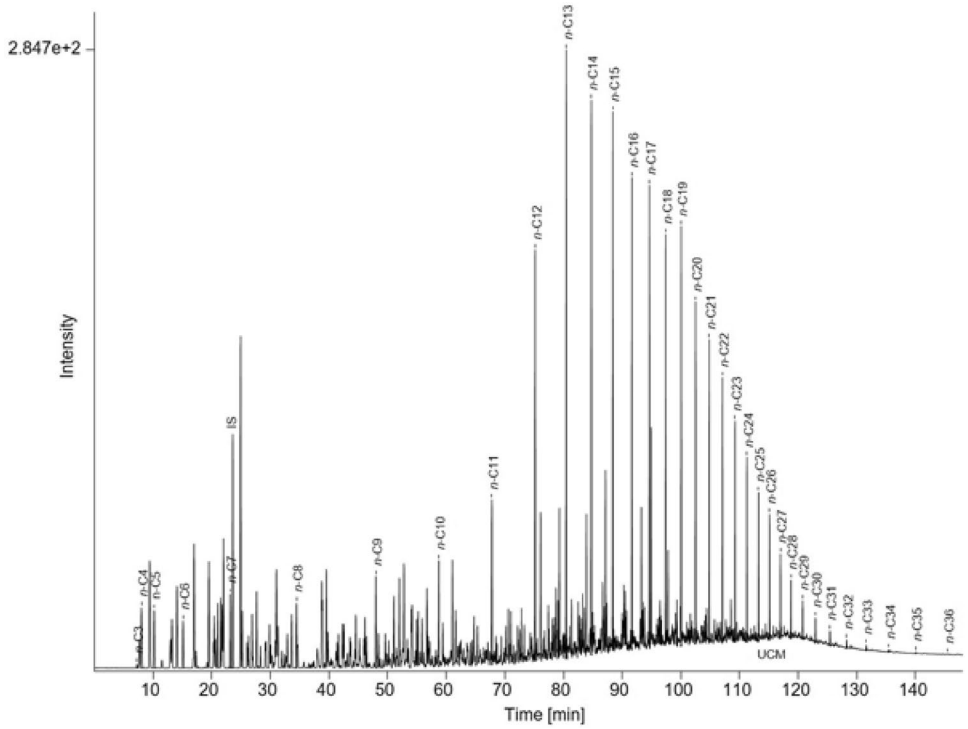

Fig. 5 Whole oil chromatogram from borehole 01-11C in Siljan impact structure. The *n*-alkanes are marked by *n*-C_x, where x represents the respective carbon number. IS is the internal standard, UCM is an unresolved complex mixture hump

The oil sample headspace gas contained 0.09% methane, 0.13% ethane, and 1.9% propane with $\delta^{13}C$ values of −56.8, −35.3, and −28.6‰, respectively. The carbon isotope values of iso-butane and n-butane were −28.9 and −27.7‰. The hydrogen isotope value of methane (δD_{CH4}) was −321‰.

3.3 Hydrogeochemistry

The groundwater in PB2 (data in Supplementary Table 2) had high alkalinity (713 mg L^{-1} $CaCO_3$), low SO_4 (20 mg L^{-1}), and Cl and Mg concentrations of 1100 mg L^{-1} and 36 mg L^{-1}, respectively. The Na concentration was 654 mg L^{-1}, Ca concentration was 149 mg L^{-1} and Br was below detection limit (< 1 mg L^{-1}). The PB2 groundwater temperature was 14.3 °C and the total dissolved solids (TDS) was 2858 mg L^{-1}. The δD_{H2O} value was −87.9‰ and the $\delta^{18}O_{H2O}$ value was −12.4‰, plotting close to the global meteoric water line (Fig. 6, GMWL, [49]).

Table 3 Molecular indices of the oil from borehole 01-11C in the Siljan impact structure

Index	Ratio	Value
n-C_7/$MCyC_6$	n-Heptane/methylcyclohexane	0.20
Tol/n-C_7	Toluene/n-heptane	0.34
Pr/n-C_{17}	Pristane/n-heptadecane	0.56
Ph/n-C_{18}	Phytane/n-octadecane	0.29
Tr1	Toluene/1,1-dimethylcyclopentane	0.75
Tr2	n-Heptane/1,1-dimethylcyclopentane	2.22
Tr3	3-Methylhexane/1,1-dimethylcyclopentane	2.11
Tr4	2-Methylhexane/1,1-dimethylcyclopentane	0.83
Tr5	2-Methylhexane + 3methylhexane/1,1-dimethylcyclopentane	2.94
Tr6	1-Cis-2-dimethylcyclopentante/1,1-dimethylcyclopentane	0
Tr7	1-Trans-3-dimethylcyclopentane/1,1-dimethylcyclopentane	2.12

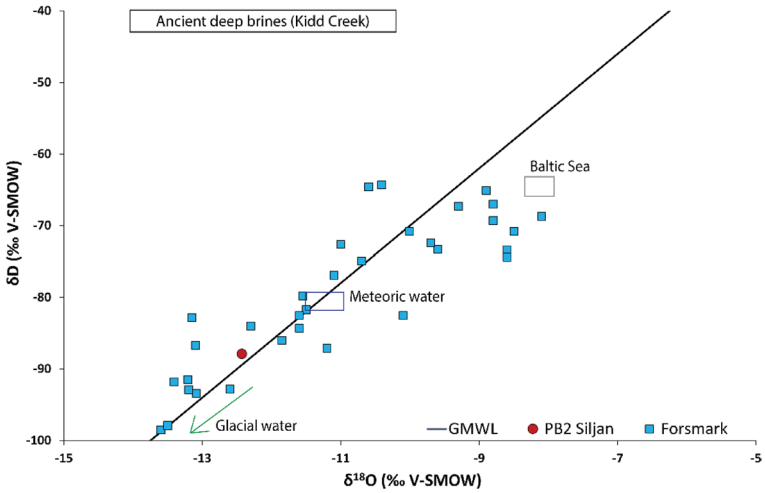

Fig. 6 Stable isotope composition (δD vs $\delta^{18}O$) in the PB2 Siljan groundwater plotted together with the Global Meteoric Water Line (GMWL), with data from another site on the Fennoscandian Shield (Forsmark) and possible end-members of Baltic Sea water, glacial waters [50] and ancient brine (Kidd Creek, Canada [51]). The local meteoric water in central Sweden at present is around -11 ± 1‰V-SMOW $\delta^{18}O_{H2O}$ for surface waters (IAEA/WMO, 2024)

3.4 Microbiology

The qPCR data gave archaeal cell abundances of 0 ± < 1.0, 1.4 ± 0.6, and 1.7 ± 0.6 16S rRNA gene copies mL^{-1} for the three biological replicate filters. Since the archaeal abundance was so low, archaeal specific primers could not be used to characterize the microbial communities in the groundwater. Despite this limitation, some archaea were identified in the groundwater communities with the bacterial primers (archaeal phylum Halobacteriota). The deep groundwater communities were dominated by Patescibacteria (> 60%) and Bacteriodota (Fig. 7a) while methanogenic archaea comprised 0.2, 3.1, and 0.5% of the relative abundance in the three replicate filters (Fig. 7b).

4 Discussion

4.1 Origin of the gas

The $\delta^{13}C_{CH4}$ values, $C_1/(C_2 + C_{3+})$ ratios, and δD_{CH4} of the free gas samples taken from boreholes PB1, PB2, and PB4 at the Siljan impact crater plot at the border of the early mature thermogenic and the microbial fields (overlapping into primary and secondary microbial fields) in the discrimination plots from Milkov and Etiope [39], indicating a mixture of thermogenic and microbial origins for methane. The carbon isotopes of CO_2 point more distinctly towards a dominantly microbial origin for PB1 and PB2, in primary microbial carbonate reduction field, bordering to secondary microbial field (Fig. 2c). In contrast, the PB4 sample indicated a more mixed thermogenic and primary microbial origin

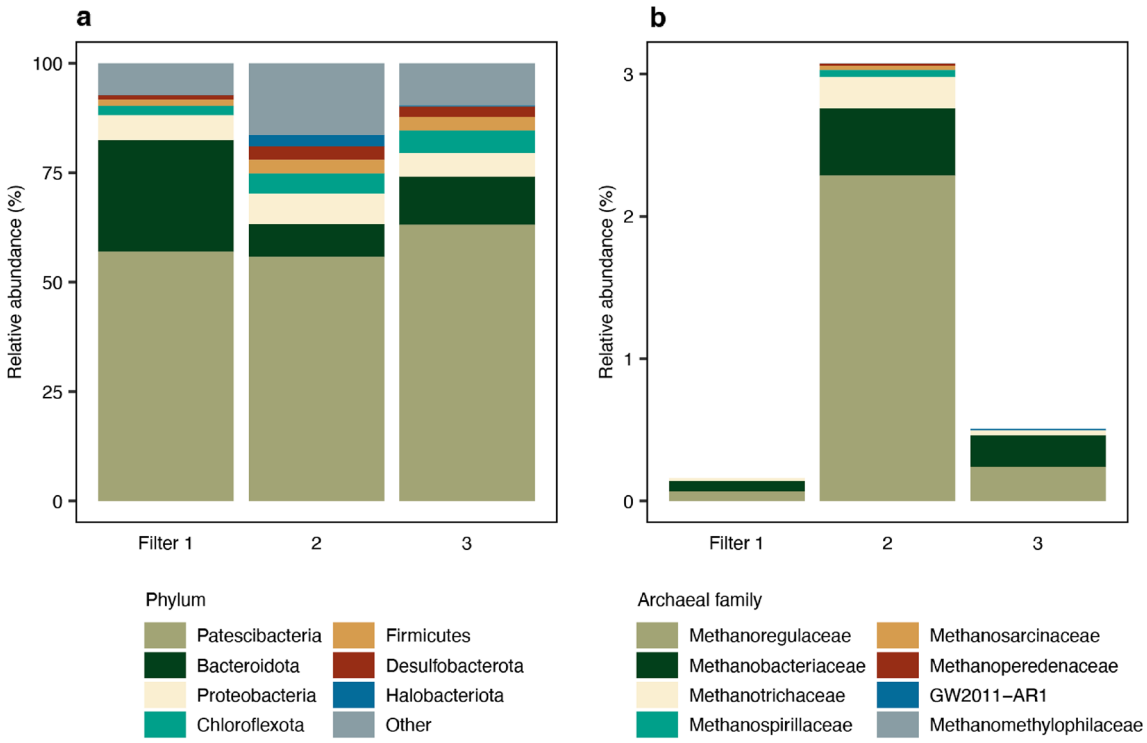

Fig. 7 **a** 16S rRNA gene based relative abundance in the PB2 groundwater at 380 m depth; **b** 16S rRNA gene based relative abundance of the archaeal phylum Halobacteriota (as part ofthe 'other' phyla in panel a for filters 1 and 3, as it constitutes < 1% of the community relative abundance)

based on the $\delta^{13}C_{CO2}$ (Fig. 2c). The relatively high CO_2 concentration in PB1 and PB2 was also indicative of carbonate reduction pathway and/or secondary microbial origin [17, 52], whereas the low concentrations of CO_2 and lower $\delta^{13}C_{CO2}$ values in PB4 potentially indicated a larger thermogenic than microbial contribution in PB4. However, CO_2 values could also partly be effected by air contamination as indicated by the relatively high O_2 + Ar values (Table 1). A thermogenic contribution to the gas was expected as bitumen, oil seeps, and shales (e.g., the organic rich Upper Ordovician Fjäcka Shale, a source rock known for economic accumulation of oil in the eastern Baltic region) are present in this formation [14]. In summary, for PB1 and PB2, the substantial ^{13}C-enrichment in CO_2 together with low $\delta^{13}C_{CH4}$ and high C_1/C_{2+} ratios, all pointed to a dominant microbial contribution to the gas mix, which also included a precursor early mature thermogenic endmember to a lesser extent.

The apparent formation temperatures derived from the $\Delta^{13}CH_3D$ (87–122 °C) were anomalously high for recently formed methane at the current depth of sampling (380 m) where the groundwater temperatures were ~ 14.3 °C (PB2). A geothermal gradient of 15–20 °C/km is plausible for this setting [53, 54] and would imply formation depths of 4.4–8.1 km. However, this was unrealistic except potentially during foreland basin formation in the aftermath of the Caledonian orogeny (~ 400–380 Ma), when sedimentary cover pushed the craton to depths of more than 4 km in the central Fennoscandian Shield [55]. If the methane was produced more recently, following uplift/denudation, it can be assumed that the high apparent temperatures were a result of kinetic fractionation during microbial methanogenesis. As microbial methanogenesis is not an equilibrium process, the clumped isotopologue compositions corresponded to anomalously high apparent equilibrium temperatures [29, 45]. Methane isotopologues can be equilibrated by microbial methanogenesis or anaerobic methane oxidation below about 60 °C or abiotically at a temperature above about 160 °C (e.g., [44, 56]). The calculated range of apparent temperature of 87 to 122 °C, suggested that the methane did not experience temperatures above 160 °C or anaerobic methane oxidation. Therefore, the apparent temperatures derived from $\Delta^{13}CH_3D$ at least partially indicated methane formation by microbial methanogenesis. Overall, the methane stable isotopes pointed towards a mixed thermogenic and microbial gas, and the disequilibrium temperatures supported a microbial methanogenesis as origin.

4.2 Biodegradation features

4.2.1 Gas

The C_1 to C_4 carbon isotopic ratios plotted against reciprocal carbon number 1/n (Fig. 8) indicated the gas had undergone biodegradation. This was evident from the propane carbon isotopic composition, as propane, n-butane, and pentane are more affected by microbial oxidation compared to ethane [57–61]. When free gas from PB1, 2, and 4 was compared to hypothetical unaltered thermogenic gas (stippled line in Fig. 8), there was a clear elevation in the $\delta^{13}C_{CH4}$ values of propane, and lesser so for ethane, which was in accordance with Kim et al. [44].

Furthermore, when comparing the free gas from the boreholes to the oil-associated gas, there was a more than 10‰ difference in the propane $\delta^{13}C$ values (Fig. 8). The propane from the oil was not as affected by microbial consumption compared to the gas from PB1, 2, and 4. The *i*-C_4/*n*-C_4 ratio of the oil-associated gas (0.85) was much lower than in PB1, 2 and 4 (1.76, 6.75 and 9.3, respectively). As *n*-C_4 is more susceptible to biodegradation than *i*-C_4 [52, 62–64], it indicated that the free gas in the boreholes has undergone biodegradation. This confirmed that biodegradation of precursor hydrocarbons was an important microbial process in this deep aquifer.

4.2.2 Oils

The presence of an UCM hump in the whole oil chromatogram indicated biodegradation of the oil, as well as the elevated *i*-C_4/*n*-C_4 ratio, as biodegradation would affect *n*-alkanes more than isoprenoids (e.g., [65–67]). The low *n*-C_7/$MCyC_6$ ratio and low TR1 to Tr7 ratios are also indicative of biodegradation [68]. Alteration of the light hydrocarbons by water washing that is often observed in combination with biodegradation, also occurred, which is indicated by the low Tol/*n*-C_7 and Tr1 [66, 67]. In contrast, the low asphaltene and high saturate contents, as well as the low Pr/*n*-C_{17} and Ph/*n*-C_{18} ratios do not suggest biodegradation.

Ahmed et al. [14] characterized seep oil and bitumens in the Siljan area from the east side of the impact crater, and those show moderate to heavy biodegradation, albeit with a high variability in maturity in different samples. The variability in the different oil samples they reported, together with the features observed in this study, indicates different oil charges. The oils in the Siljan impact structure likely represented mixtures of biodegraded and non-biodegraded oils.

4.3 Hydrological origin and influence on methanogenesis

The stable hydrogen and oxygen isotopic compositions of the groundwater follow the GMWL (Fig. 6). In systems with prolonged water–rock interaction at low water to rock ratios, such as old continental brines in South Africa, Canada, and the Fennoscandian Shield [48, 69, 70], the values will diverge from the GMWL with time. The Siljan sample was thus interpreted to be dominated by meteoric water with limited water–rock interaction. However, the oxygen isotope value (−12.4‰ V-SMOW $\delta^{18}O_{H2O}$) was slightly lower, although overlapping, with modern meteoric water in the Siljan area (−11 ± 1‰ V-SMOW for surface waters, IAEA/WMO (2024)), which might indicate a small contribution from at least one other meteoric source water. Considering that glacial meltwater has low $\delta^{18}O$ values (−21 to −16‰V-SMOW, [50]), a Late Pleistocene glacial meltwater endmember may be a plausible mixing endmember that can explain the relatively low $\delta^{18}O$

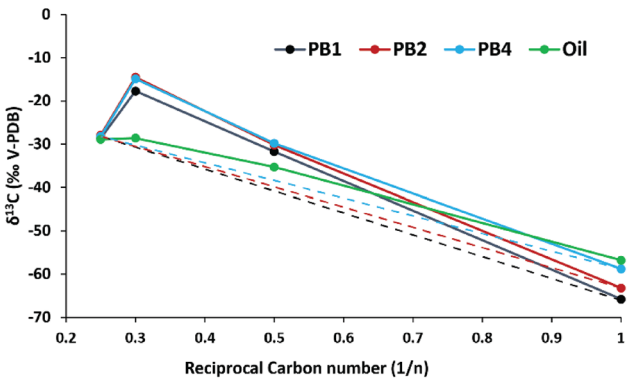

Fig. 8 Reciprocal carbon numbers of the three boreholes and comparison with oil-associated gas, indicating biodegradation. Dashed lines indicate the isotopic values without alteration

values detected. However, the salinity indicated by chlorine concentration (1100 mg L^{-1}) was not fully compatible with meteoric or glacial water origins, and requires a third, more saline source in the mix. Therefore, mixing with deep saline water or a relict marine water may have occurred, which are commonly encountered at depth in the Fennoscandian Shield [50, 71, 72]. The Mg concentrations of 36 mg L^{-1} was more indicative of marine contribution as deep saline water usually has concentrations below 3 mg L^{-1} and marine waters can have up to ~ 450 mg L^{-1} [72]. The expected Br concentration based on the Cl concentration (1100 mg L^{-1}) and a Br/Cl ratio typical for seawater (0.0035, [73]) would be around 3.8 mg L^{-1}. The Br concentration being below detection (< 0.1 mg L^{-1}) inferred that the saline endmember was not dominantly from a marine source, but instead indicated a significant deep saline fraction to the saline endmember. Although the residence time of the water was unknown, it can thus be proposed that the waters at 380 m depth in the PB2 borehole were relatively recently infiltrated, i.e., after sedimentary covers have been eroded in the Cenozoic [74] and freshwater infiltration was enabled (such as during Quaternary deglaciations and/or from subglacial recharge). If the residence time of the groundwater was longer, and the groundwater was isolated, a higher concentration of helium would be expected, as seen for instance in Outokumpu, Finland [70, 75]. As the helium content was low (< 0.04%) in an otherwise gas-rich formation, this supported a more recent infiltration of water. Overall, the source of the groundwater was likely dominantly meteoric, from a relatively recent infiltration, with a smaller component of marine and/or glacial waters.

The sulfate concentration of 20 mg L^{-1} was lower than in many deep saline and marine waters infiltrated during transgressions in the Fennoscandian Shield (~ 200–1000 mg L^{-1}, [50, 76]), but in line with meteoric or glacial waters. Methanogens are associated with lower sulfate concentrations, because at higher sulfate concentrations, they are outcompeted by sulfate reducing bacteria (SRB) for acetate and hydrogen [77], which has also been indicated in natural systems influenced by dilute water infiltration [78, 79]. The PB2 sulfate concentration (20 mg L^{-1} = 208 µM) was close to the sulfate threshold where bacterial sulfate reduction can become the dominant carbon reducing pathway (~ 100 µM, [80]).

The abundant sub-vertical fracture zones associated with the impact ring structure may have been particularly influential in allowing meteoric waters to infiltrate to ~ 400 m depth. The presence of earlier formed thermogenic gas and oil could have provided organic carbon that could be degraded initially during sulfate reduction, leading to microbial conversion of hydrocarbons to biomass and carbon dioxide providing substrate for methanogenesis [81–84]. The carbon dioxide produced was likely further reduced to methane using molecular hydrogen [60].

The high alkalinity detected in PB2 groundwater can be a further indicator of in situ microbial methanogenesis [85], but could also reflect other microbial processes, such as sulfate reduction. Taken together, it is plausible that microbial methane generation in this setting was triggered by dilution of deeper saline water through the infiltration of meteoric waters that led to lowering of the sulfate concentration, potentially aided by SRB initiating biodegradation of the primary hydrocarbons, creating suitable conditions for methanogens.

4.4 Microbiological pathways for methanogenesis

Taking the thermogenic mixing endmember aside, the discrimination plots (Fig. 2) indicated microbial methanogenesis through various pathways depending on which proxy was used. Although the relatively low $\delta^{13}C_{CH4}$ and the relatively high $C_1/(C_2+C_{3+})$ point in the direction of carbonate reduction pathway and/or being formed by secondary microbial degradation of precursor hydrocarbons [39],Vinson et al. [86] showed that the fractionation between δD_{CH4} and δD_{H2O} can indicate an apparent hydrogenotrophic pathway, regardless of the actual metabolic pathway generating the methane. This is caused by equilibration of the H isotopes between methane precursors and the groundwater. When the Siljan free gas sample PB2 with corresponding water sample was plotted in the δD_{CH4} vs δD_{H2O} diagram (Fig. 9), it positions just on the left side of hydrogenotrophic methanogenesis. However, this does not exclude a methylotrophic or acetoclastic pathway.

The presence of several methanogenic archaeal families in the groundwater indicated multiple methanogenesis pathways. The relative abundance of methanogens was low, but the abundance cannot be certain due to PCR primer bias. Moreover, Tong et al. [87] found only a weak correlation between methane production and abundance of methanogens, indicating a small abundance of methanogens can still produce methane, if enough substrate is available. The most abundant family was Methanoregulaceae, of which its members are reported to mainly use CO_2-hydrogenotrophic pathways [88] or using formate and hydrogen for growth and methane production [89]. The second most abundant family was Methanobacteriaceae from the Methanobacteriales order that is ubiquitous in many different environments [90]. This family predominantly consists of CO_2-reducing hydrogenotrophic methanogens [90] with fewer methylotrophic methanogen taxa [91]. *Methanospirullum* from the Methanospirrillaceae is also mainly hydrogenotrophic or can use formate and hydrogen [92]. Methanothrix was also present in all three DNA samples, an obligate acetoclastic methanogen that

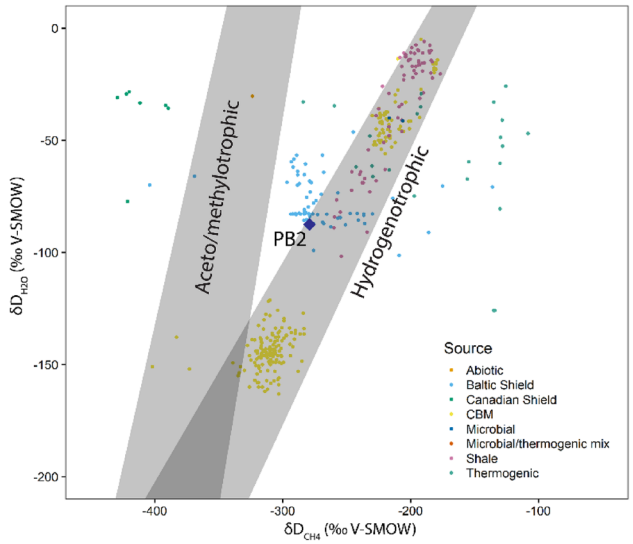

Fig. 9 Hydrogen isotope ratios of methane and the host groundwater, with inferred lines for hydrogenotrophic and acetoclastic/methylotrophic methanogenesis [86]. CBM = Coal Bed Methane

is unable to grow on CO_2 or formate [93]. Methanosarcinaceae are one of the most diverse methanogenic families, being able to use methylated compounds, acetate, and CO_2 [90]. Methanogens of the Methanomethylophilaceae family are predominantly obligate methylothrophs, reducing methyl groups using H_2 as the electron donor, and have been found mostly in the animal digestive tract [94]. Co-occurring in low abundance with the methanogens was the methanotrophic archaeal family Methanoperedenaceae. Finally, Leu et al. [95] show that members of the family Methanoperedenaceae (formerly known as ANME-2d) are capable of the anaerobic oxidation of methane coupled to nitrate and iron reduction.

In summary, microbial methane in the Siljan impact crater likely originated via predominantly CO_2 reduction, as well as methylotrophic and acetoclastic methanogenic pathways, and mixed with pre-existing thermogenic gas that originates from the shales (such as Fjäcka shale) in the sedimentary successions. However, the methanogens were present in low abundances and not all species could be detected in the sequencing. Furthermore, other methanogens may be present that will further convolute potential methanogenesis pathways [87].

4.5 Conditions for microbial methane formation in meteorite impact craters, and comparison to other settings

The Siljan impact structure is, to the best or our knowledge, the only known crater on Earth with significant microbial methane seepage. The reports of seeping methane of unknown origin in the Gale crater on Mars [4], make the Siljan impact crater a terrestrial analogue. To put the formation conditions of microbial methane at Siljan into context, we will compare it to other sites with sedimentary basins where microbial methane accumulates, the Michigan Basin and the Illinois Basin, USA.

The Michigan Basin contains a Devonian black shale (Antrim Shale) within sedimentary strata, and its gas production is of economic importance. Both microbial and thermogenic gas has been identified, but microbial gas dominates. Martini et al. [96] presented a comprehensive data set on the gas produced from the Antrim Shale. The $\delta^{13}C$ of methane ranges from −57.9 to −43.0‰, with the former being indicative of an immature thermogenic gas, and this gas being diluted by variable amounts of microbial gas. The methane gas has a lower than typical isotopic signature for microbial gas, but high $C_1/(C_2+C_3)$ ratio (149 to 257) at the western margin is indicative of microbial gas. The microbial gas deposits are located where there is a permeable fracture network allowing for fresh water to infiltrate, which is at the margin of the basin.

The Illinois Basin is underlain by Precambrian bedrock, overlain by the Devonian New Albany Shale and Paleozoic sedimentary rocks. Microbial methane accumulations are present in the New Albany Shale, with $\delta^{13}C_{CH4}$ ranging between −65.4 to −57.9‰ and $\delta^{13}C_{CO2}$ values of 0.1 to 6.6‰ [97], similar to the isotopic composition of the Siljan free gas. Strąpoć et al. [98, 99] found $\delta^{13}C_{CH4}$ ranging between −65.1 and −56.6‰ and concludes that high permeability allows inoculation of methanogenic consortia, leading to microbial methane generation in eastern margin of Illinois Basin. The geochemical conditions reported in the Illinois Basin by Schlegel et al. [100], such as neutral pH, low sulfate concentrations (< 2 mM) and $Cl^- < 3$ M, are favorable for methanogenic microbes. Additionally, low numbers of archaea species were identified, likely methanogenic. Strąpoć et al. [99] characterized the methanogenic microbes in the Illinois Basin,

with *Methanocorpusculum* as the dominant genus, which has also been found in the Michigan Basin [101]. However, as different 16S rRna gene PCR primers were used, comparison to our dataset is difficult.

Based on data from the Michigan Basin, Martini et al. [96] described the optimal conditions for microbial gas and microbial colonization, such as dilute formation water (< 3 M Cl^-) with low sulfate concentrations (< 0.05 mM), increased reservoir permeability via high density of fracture networks in shales, high CO_2 concentrations (> 2%) in the gas and high $\delta^{13}C_{CO2}$ values (> 10‰). The $\delta^{13}C_{CO2}$ is lower (> 5‰) in the Siljan impact crater, but all other conditions are met.

Taken together, this all suggested that the microbial methane accumulation in the Siljan impact crater shows great similarities to sedimentary basins and its conditions and occurred through similar mechanisms. The presence of shale and organic matter, the meteoric water containing low sulfate and Cl^- concentrations, and the highly fractured nature of the Siljan impact structure was apparently optimal for the promoting microbial methanogenesis. The Siljan impact crater is of interest as an analogue for determining the source of microbial methane gas in other impact craters, both on Earth and on other planetary bodies, but as we show, its nature is highly influenced by terrestrial organic rich shales, and a complex history of late-stage infiltration of surface water.

5 Conclusions

Based on conventional stable isotope analysis and multiply substituted isotopologues, the methane present at several hundred meters depth in the fracture aquifer of the Siljan impact crater was characterized to be of mixed thermogenic and microbial origin. The microbial methanogenesis occurred in a coupled system, where sulfate reducers performed anaerobic oxidation of hydrocarbons (ethane and oil) to produce CO_2, which was then used by methanogens to produce methane. Recharge with relatively sulfate poor freshwater coupled with bacterial sulfate reduction lowered the dissolved sulfate concentration to levels preventing methanogens from being outcompeted by sulfate reducers. The presence of multiple methanogen populations suggested to generate methane via different pathways indicated a complex methanogenesis system with multiple pathways and is the first report of modern methanogenesis in a deeply fractured impact structure on Earth. In addition to these new models for methane formation in this unusual petroleum system, there are astrobiological implications that include Earth analogue evidence of deep microbial colonization of porous and highly fractured target rock of an impact structure, with associated microbial methane accumulation and seepage.

Acknowledgements Financial support was received from a Swedish Research Council FORMAS grant (2020-01577 to Drake and Dopson), a Swedish Research Council grant (2021-04365 to Drake), J. Gust. Richert foundation grant (to Drake), Crafoord foundation grant (20210524 to Drake), NSF FRES SMRFS grant (EAR 2120733 to McIntosh and Drake), Swedish Research Council (2018-04311 to Dopson) and German Research Council (DFG RE 5345/1-1 to Reinhardt). High-throughput sequencing was carried out at the National Genomics Infrastructure hosted by the Science for Life Laboratory, Sweden. Bioinformatics analyses were carried out utilizing the Uppsala Multidisciplinary Center for Advanced Computational Science (UPPMAX) at Uppsala University (NAISS 2023/22-893 and 2023/6-261). The computations were enabled by resources provided by the National Academic Infrastructure for Supercomputing in Sweden (NAISS) and the Swedish National Infrastructure for Computing (SNIC) at UPPMAX, Uppsala University, partially funded by the Swedish Research Council through grant agreement nos. 2022-06725 and 2018-05973. Arto Pullinen (GTK) and Magnus Ståhle (LNU) are thanked for assisting in the field and Mia Tiljander (GTK) for water stable isotope analysis.

Author contributions Conceptualization: F.v.D, H.D.; Funding acquisition: H.D., J.M.; Field work: F.v.D., H.D., R.K., M.D.; Formal analysis: F.v.D., H.D., S.O., R.K., M.K., M.R., G.W.; Visualization: F.v.D., G.W.; Writing – original draft: F.v.D, H.D.; Writing – review & editing: F.v.D., H.D., S.O., R.K., M.K., M.R., G.W., M.D., J.M.

Funding Open access funding provided by Linnaeus University.

Data availability Data is provided within the manuscript or supplementary information files.

Code availability Not applicable.

Declarations

Competing interest The authors declare no competing interests.

References

1. Osinski GR, Cockell CS, Pontefract A, Sapers HM. The role of meteorite impacts in the origin of life. Astrobiology. 2020;20(9):1121–49. https://doi.org/10.1089/ast.2019.2203.
2. Cockell CS. The origin and emergence of life under impact bombardment. Philos Trans R Soc B: Biol Sci. 2006;361(1474):1845. https://doi.org/10.1098/RSTB.2006.1908.
3. Cockell CS, Lee P. The biology of impact craters: a review. Biol Rev. 2002;77:279–310. https://doi.org/10.1017/S146479310100584X.
4. Webster CR, et al. Mars methane detection and variability at Gale crater. Science. 2015;347(6220):415–7. https://doi.org/10.1126/SCIENCE.1261713/SUPPL_FILE/WEBSTER.SM.PDF.
5. Krasnopolsky VA, Maillard JP, Owen TC. Detection of methane in the martian atmosphere: evidence for life? Icarus. 2004;172(2):537–47. https://doi.org/10.1016/J.ICARUS.2004.07.004.
6. Jourdan F, Reimold WU, Deutsch A. Dating terrestrial impact structures. Elements. 2012;8(1):49–53. https://doi.org/10.2113/GSELEMENTS.8.1.49.
7. Juhlin C, Sturkell E, Ebbestad JOR, Lehnert O, Högström AES, Meinhold G. A new interpretation of the sedimentary cover in the western Siljan Ring area, central Sweden, based on seismic data. Tectonophysics. 2012;580:88–99. https://doi.org/10.1016/J.TECTO.2012.08.040.
8. Merriam DF. Linnaeus' 1734 Dalaresa and His Geological Observations. Trans Kansas Acad Sci. 1992;95:211.
9. Gold T, Soter S. Abiogenic methane and the origin of petroleum. Energy Explor Exploit. 1982;1(2):89–104. https://doi.org/10.1177/014459878200100202.
10. Drake H, et al. Timing and origin of natural gas accumulation in the Siljan impact structure, Sweden. Nat Commun. 2019;10(1):1–14. https://doi.org/10.1038/s41467-019-12728-y.
11. Hode T, Cady SL, von Dalwigk I, Kristiansson P. Evidence of ancient microbial life in an impact structure and its implications for astrobiology. In: From Fossils to Astrobiology Cellular Origin, Life in Extreme Habitats and Astrobiology. 2009;12:249–73. https://doi.org/10.1007/978-1-4020-8837-7_12.
12. Siljeström S, Hode T, Lausmaa J, Sjövall P, Toporski J, Thiel V. Detection of organic biomarkers in crude oils using ToF-SIMS. Org Geochem. 2009;40(1):135–43. https://doi.org/10.1016/J.ORGGEOCHEM.2008.08.010.
13. Siljeström S, Lausmaa J, Sjövall P, Broman C, Thiel V, Hode T. Analysis of hopanes and steranes in single oil-bearing fluid inclusions using time-of-flight secondary ion mass spectrometry (ToF-SIMS). Geobiology. 2010;8(1):37–44. https://doi.org/10.1111/J.1472-4669.2009.00223.X.
14. Ahmed M, Lehnert O, Fuentes D, Meinhold G. Origin of oil and bitumen in the Late Devonian Siljan impact structure, central Sweden. Org Geochem. 2014;68:13–26. https://doi.org/10.1016/j.orggeochem.2013.12.010.
15. Vlierboom F, Collini B, Zumberge J. The occurrence of petroleum in sedimentary rocks of the meteor impact crater at Lake Siljan, Sweden. Org Geochem. 1986;10(1–3):153–61.
16. Drake H, et al. Fossilized anaerobic and possibly methanogenesis-fueling fungi identified deep within the Siljan impact structure, Sweden. Commun Earth Environ. 2021;2(1):1. https://doi.org/10.1038/s43247-021-00107-9.
17. Whiticar MJ. Carbon and hydrogen isotope systematics of bacterial formation and oxidation of methane. Chem Geol. 1999;161(1):291–314. https://doi.org/10.1016/S0009-2541(99)00092-3.
18. Miettinen H, Kietäväinen R, Sohlberg E, Numminen M, Ahonen L, Itävaara M. Microbiome composition and geochemical characteristics of deep subsurface high-pressure environment Pyhäsalmi mine Finland. Front Microbiol. 2015;6:1203. https://doi.org/10.3389/fmicb.2015.01203.
19. Fredrickson JK, Balkwill DL. Geomicrobial processes and biodiversity in the deep terrestrial subsurface. Geomicrobiol J. 2006;23(6):345–56. https://doi.org/10.1080/01490450600875571.
20. Ino K, et al. Deep microbial life in high-quality granitic groundwater from geochemically and geographically distinct underground boreholes. Environ Microbiol Rep. 2016;8(2):285–94. https://doi.org/10.1111/1758-2229.12379.
21. Wani AA, et al. Molecular analyses of microbial diversity associated with the Lonar soda lake in India: an impact crater in a basalt area. Res Microbiol. 2006;157(10):928–37. https://doi.org/10.1016/J.RESMIC.2006.08.005.
22. Maltais MJ, Vincent WF. Periphyton community structure and dynamics in a subarctic lake. Can J Bot. 1997;75(9):1556–69. https://doi.org/10.1139/B97-868.
23. Cockell CS, et al. Microbial abundance in the deep subsurface of the Chesapeake Bay impact crater: Relationship to lithology and impact processes. In: The ICDP-USGS Deep Drilling Project in the Chesapeake Bay impact structure: Results from the Eyreville Core Holes Geological Society of America. 2009. https://doi.org/10.1130/2009.2458(40).
24. Cockell CS, et al. Shaping of the present-day deep biosphere at chicxulub by the impact catastrophe that ended the cretaceous. Front Microbiol. 2021;12:1. https://doi.org/10.3389/fmicb.2021.668240.
25. Martini AM, Walter LM, Ku TCW, Budai JM, McIntosh JC, Schoell M. Microbial production and modification of gases in sedimentary basins: a geochemical case study from a Devonian shale gas play, Michigan basin. Am Assoc Pet Geol Bull. 2003;87(8):1355–75. https://doi.org/10.1306/031903200184.
26. McIntosh J, et al. Burial and denudation alter microbial life at the bottom of the hypo-critical zone. Geochem Geophys Geosyst. 2023;24(6):1. https://doi.org/10.1029/2022GC010831.

27. McIntosh JC, Walter LM, Martini AM. Pleistocene recharge to midcontinent basins: effects on salinity structure and microbial gas generation. Geochim Cosmochim Acta. 2002;66(10):1681–700. https://doi.org/10.1016/S0016-7037(01)00885-7.
28. Ward JA, et al. Microbial hydrocarbon gases in the Witwatersrand Basin, South Africa: Implications for the deep biosphere. Geochim Cosmochim Acta. 2004;68(15):3239–50. https://doi.org/10.1016/J.GCA.2004.02.020.
29. Wang DT, et al. Nonequilibrium clumped isotope signals in microbial methane. Science (1979). 1979;348(6233):2015.
30. Ono S, et al. Measurement of a doubly substituted methane isotopologue, $^{13}CH_3D$, by tunable infrared laser direct absorption spectroscopy. Anal Chem. 2014;86(13):6487–94. https://doi.org/10.1021/AC5010579.
31. Eldridge DL, et al (2019) Comparison of Experimental vs Theoretical Abundances of $^{13}CH_3D$ and $^{12}CH_2D_2$ for Isotopically Equilibrated Systems from 1 to 500 °C. In: ACS Publications, DL Eldridge, R Korol, MK Lloyd, AC Turner, MA Webb, TF Miller III, DA Stolper (eds) ACS Earth and Space Chemistry, vol 3(12), 2747–2764. ACS Publications. https://doi.org/10.1021/acsearthspacechem.9b00244.
32. Lopez-Fernandez M, Åström M, Bertilsson S, Dopson M. Depth and dissolved organic carbon shape microbial communities in surface influenced but not ancient saline terrestrial aquifers. Front Microbiol. 2018;9:1. https://doi.org/10.3389/FMICB.2018.02880.
33. Herlemann DPR, Labrenz M, Jürgens K, Bertilsson S, Waniek JJ, Andersson AF. Transitions in bacterial communities along the 2000 km salinity gradient of the Baltic Sea. ISME J. 2011;5(10):1571–9. https://doi.org/10.1038/ismej.2011.41.
34. Yu Y, Lee C, Hwang S. Analysis of community structures in anaerobic processes using a quantitative real-time PCR method. Water Sci Technol. 2005;52(1–2):85–91. https://doi.org/10.2166/WST.2005.0502.
35. Straub D, Blackwell N, Langarica-Fuentes A, Peltzer A, Nahnsen S, Kleindienst S. Interpretations of environmental microbial community studies are biased by the selected 16S rRNA (Gene) amplicon sequencing pipeline. Front Microbiol. 2020;11: 550420. https://doi.org/10.3389/FMICB.2020.550420/BIBTEX.
36. Ewels PA, et al. The nf-core framework for community-curated bioinformatics pipelines. Nat Biotechnol. 2020;38(3):276–8. https://doi.org/10.1038/s41587-020-0439-x.
37. Lundin D, Andersson A. SBDI Sativa curated 16S GTDB database. FigShare. https://doi.org/10.17044/scilifelab.14869077.v6.
38. Westmeijer G, et al. Continental scientific drilling and microbiology: (extremely) low biomass in bedrock of central Sweden. Biogeosciences. 2024;21(2):591–604. https://doi.org/10.5194/BG-21-591-2024.
39. Milkov AV, Etiope G. Revised genetic diagrams for natural gases based on a global dataset of >20,000 samples. Org Geochem. 2018;125:109–20. https://doi.org/10.1016/j.orggeochem.2018.09.002.
40. Taylor SW, Lollar BS, Wassenaar LI. Bacteriogenic ethane in near-surface aquifers: Implications for leaking hydrocarbon well bores. Environ Sci Technol. 2000;34(22):4727–32. https://doi.org/10.1021/ES001066X/ASSET/IMAGES/MEDIUM/ES001066XE00002.GIF.
41. Douglas PMJ, et al. Diverse origins of Arctic and Subarctic methane point source emissions identified with multiply-substituted isotopologues. Geochim Cosmochim Acta. 2016;188:163–88. https://doi.org/10.1016/J.GCA.2016.05.031.
42. Young ED, et al. The relative abundances of resolved $^{12}CH_2D_2$ and $^{13}CH_3D$ and mechanisms controlling isotopic bond ordering in abiotic and biotic methane gases. Geochim Cosmochim Acta. 2017;203:235–64. https://doi.org/10.1016/J.GCA.2016.12.041.
43. Giunta T, et al. Methane sources and sinks in continental sedimentary systems: New insights from paired clumped isotopologues $^{13}CH_3D$ and $^{12}CH_2D_2$. Geochim Cosmochim Acta. 2019;245:327–51. https://doi.org/10.1016/J.GCA.2018.10.030.
44. Kim JH, Martini AM, Ono S, Lalk E, Ferguson G, McIntosh JC. Clumped and conventional isotopes of natural gas reveal basin burial, denudation, and biodegradation history. Geochim Cosmochim Acta. 2023;361:133–51. https://doi.org/10.1016/J.GCA.2023.10.017.
45. Stolper DA, et al. Distinguishing and understanding thermogenic and biogenic sources of methane using multiply substituted isotopologues. Geochim Cosmochim Acta. 2015;161:219–47. https://doi.org/10.1016/J.GCA.2015.04.015.
46. Stolper DA, et al. Formation temperatures of thermogenic and biogenic methane. Science. 2014;344(6191):1500–3. https://doi.org/10.1126/SCIENCE.1254509.
47. Lin YT, et al. Diverse origins of gases from mud volcanoes and seeps in tectonically fragmented terrane. Geochem Geophys Geosyst. 2023;24(10):1. https://doi.org/10.1029/2022GC010791.
48. Warr O, Young ED, Giunta T, Kohl IE, Ash JL, Sherwood Lollar B. High-resolution, long-term isotopic and isotopologue variation identifies the sources and sinks of methane in a deep subsurface carbon cycle. Geochim Cosmochim Acta. 2021;294:315–34. https://doi.org/10.1016/j.gca.2020.12.002.
49. Craig H. Isotopic variations in meteoric waters. Science. 1961;133(3465):1702–3. https://doi.org/10.1126/science.133.3465.1702.
50. Gimeno MJ, Tullborg E-L, Nilsson A-C, Auqué LF, Nilsson L. Hydrogeochemical characterisation of the groundwater in the crystalline basement of Forsmark, the selected area for the geological nuclear repositories in Sweden. J Hydrol (Amst). 2023;624:129818. https://doi.org/10.1016/j.jhydrol.2023.129818.
51. Warr O, et al. Tracing ancient hydrogeological fracture network age and compartmentalisation using noble gases. Geochim Cosmochim Acta. 2018;222:340–62. https://doi.org/10.1016/j.gca.2017.10.022.
52. Pallasser RJ. Recognizing biodegradation in gas/oil accumulations through the $\delta^{13}C$ compositions of gas components. Org Geochem. 2000;31(12):1363–73. https://doi.org/10.1016/S0146-6380(00)00101-7.
53. Sundberg J, et al. Thermal data for paleoclimate calculations from boreholes at Lake Vättern. 2016, Accessed: Mar. 21, 2024. [Online]. https://skb.se/publikation/2487888/P-16-03.pdf
54. Sundberg J, Back P-E, Ländell M, Sundberg A. Svensk Kärnbränslehantering AB Modelling of temperature in deep boreholes and evaluation of geothermal heat flow at Forsmark and Laxemar. CM Gruppen AB, 2009. Accessed: March 21, 2024 (Online). www.skb.se.
55. Guenthner WR, Reiners PW, Drake H, Tillberg M. Zircon, titanite, and apatite (U-Th)/He ages and age-eU correlations from the Fennoscandian Shield, southern Sweden. Tectonics. 2017;36(7):1254–74. https://doi.org/10.1002/2017TC004525.
56. Lalk E, Velez A, Ono S. Methane clumped isotopologue variability from ebullition in a mid-latitude lake. ACS Earth Space Chem. 2024. https://doi.org/10.1021/ACSEARTHSPACECHEM.3C00282.
57. Musat F. The anaerobic degradation of gaseous, nonmethane alkanes—From in situ processes to microorganisms. Comput Struct Biotechnol J. 2015;13:222–8. https://doi.org/10.1016/J.CSBJ.2015.03.002.
58. Jaekel U, Musat N, Adam B, Kuypers M, Grundmann O, Musat F. Anaerobic degradation of propane and butane by sulfate-reducing bacteria enriched from marine hydrocarbon cold seeps. ISME J. 2012;7(5):885–95. https://doi.org/10.1038/ismej.2012.159.

59. Sassen R, et al. Free hydrocarbon gas, gas hydrate, and authigenic minerals in chemosynthetic communities of the northern Gulf of Mexico continental slope: relation to microbial processes. Chem Geol. 2004;205(3–4):195–217. https://doi.org/10.1016/J.CHEMGEO.2003.12.032.
60. Head IM, Jones DM, Larter SR. Biological activity in the deep subsurface and the origin of heavy oil. Nature. 2003;426(6964):344–52. https://doi.org/10.1038/nature02134.
61. James AT, Burns BJ. Microbial alteration of subsurface natural gas accumulations. Am Assoc Pet Geol Bull. 1984;68(8):957–60. https://doi.org/10.1306/AD46169C-16F7-11D7-8645000102C1865D.
62. Palmer SE Effect of Biodegradation and Water Washing on Crude Oil Composition. In: Engel, M.H., Macko, S.A. (eds) Organic Geochemistry. Topics in Geobiology. 1993; vol 11. Springer, Boston, MA. https://doi.org/10.1007/978-1-4615-2890-6_23.
63. Wang WC, Zhang L, Liu W, Kang Y, JR-G. Effects of biodegradation on the carbon isotopic composition of natural gas—A case study in the bamianhe oil field of the Jiyang Depression, Eastern China. J RenGeochemical J. 2005;39:301
64. Larter S, et al. When biodegradation preserves petroleum: North Sea oil rimmed gas accumulations (ORGA's). In: Abstracts of the AAPG Hedberg Research Conference "Natural gas Formation and Occurrence", Durango. 1999.
65. Tissot B, Welte D. Petroleum formation and occurrence. 2013; Accessed 08 May 2024. https://books.google.nl/books?hl=nl&lr=&id=avLxCAAAQBAJ&oi=fnd&pg=PA3&dq=Tissot,+B.P.,+Welte,+D.H.,+1984.+Petroleum+Formation+and+Occurrence.+Springer,+Berlin.%27&ots=1LY3eUk1WE&sig=GlF6vBwo1uSK_oJ3vcRFJAq9f3c
66. Wenger LM, Davis CL, Isaksen GH. Multiple controls on petroleum biodegradation and impact on oil quality. 2002.
67. Jones DM, et al. Crude-oil biodegradation via methanogenesis in subsurface petroleum reservoirs. Nature. 2007;451(7175):176–80. https://doi.org/10.1038/nature06484.
68. Halpern HI. Development and applications of light-hydrocarbon-based star diagrams. Am Assoc Pet Geol Bull. 1995;79(6):801–15.
69. Nisson DM, et al. Hydrogeochemical and isotopic signatures elucidate deep subsurface hypersaline brine formation through radiolysis driven water-rock interaction. Geochim Cosmochim Acta. 2023;340:65–84. https://doi.org/10.1016/j.gca.2022.11.015.
70. Kietäväinen R, Ahonen L, Kukkonen IT, Hendriksson N, Nyyssönen M, Itävaara M. Characterisation and isotopic evolution of saline waters of the Outokumpu Deep Drill Hole, Finland—Implications for water origin and deep terrestrial biosphere. Appl Geochem. 2013;32:37–51. https://doi.org/10.1016/j.apgeochem.2012.10.013.
71. Laaksoharju M, et al. Svensk Kärnbränslehantering AB Bedrock hydrogeochemistry Forsmark Site descriptive modelling SDM-Site Forsmark Bedrock hydrogeochemistry Forsmark-Site descriptive modelling-SDM-Site Forsmark. 2009; www.skb.se.
72. Laaksoharju M, Tullborg EL, Wikberg P, Wallin B, Smellie J. Hydrogeochemical conditions and evolution at the Äspö HRL, Sweden. Appl Geochem. 1999;14(7):835–59. https://doi.org/10.1016/S0883-2927(99)00023-2.
73. Morris AW, Riley JP. The bromide/chlorinity and sulphate/chlorinity ratio in sea water. Deep-Sea Res Oceanogr Abstr. 1966;13(4):699–705. https://doi.org/10.1016/0011-7471(66)90601-2.
74. Lidmar-Bergström KK. Long term morphotectonic evolution in Sweden. Geomorphology. 1996;16(1):33–59.
75. Kietäväinen R, Ahonen L, Kukkonen IT, Niedermann S, Wiersberg T. Noble gas residence times of saline waters within crystalline bedrock, Outokumpu Deep Drill Hole, Finland. Geochim Cosmochim Acta. 2014;145:159–74. https://doi.org/10.1016/J.GCA.2014.09.012.
76. Laaksoharju M, et al. Svensk Kärnbränslehantering AB Bedrock hydrogeochemistry Forsmark Site descriptive modelling SDM-Site Forsmark Bedrock hydrogeochemistry Forsmark-Site descriptive modelling-SDM-Site Forsmark. *CM Gruppen AB*, 2009, Accessed Mar. 13, 2024 (Online). www.skb.se.
77. Raskin L, Rittmann BE, Stahl DA. Competition and coexistence of sulfate-reducing and methanogenic populations in anaerobic biofilms. Appl Environ Microbiol. 1996;62(10):3847–57. https://doi.org/10.1128/AEM.62.10.3847-3857.1996.
78. Martini A, Walter L, Budai J, Ku T, Kaiser C, Schoell M. Genetic and temporal relations between formation waters and biogenic methane: Upper Devonian Antrim Shale, Michigan Basin, USA. Geochim Cosmochim Acta. 1998;62(10):1699–720.
79. McIntosh J, et al. Burial and denudation alter microbial life at the bottom of the Hypo-Critical Zone. Geochem Geophys Geosyst. 2023;24(6):e2022GC010831. https://doi.org/10.1029/2022GC010831.
80. Lovley DR, Klug MJ. Sulfate reducers can outcompete methanogens at freshwater sulfate concentrations. Appl Environ Microbiol. 1983;45(1):187–92. https://doi.org/10.1128/AEM.45.1.187-192.1983.
81. Zengler K, Richnow H, Rosselló-Mora R. Methane formation from long-chain alkanes by anaerobic microorganisms. Nature. 1999;401:266–9.
82. Widdel F, Rabus R. Anaerobic biodegradation of saturated and aromatic hydrocarbons. Curr Opin Biotechnol. 2001;12(3):259–76. https://doi.org/10.1016/S0958-1669(00)00209-3.
83. Wang D, et al. Geochemical evidence for secondary microbial gas in deep hot reservoirs of the Tarim Basin. Chem Geol. 2022;587: 120630. https://doi.org/10.1016/J.CHEMGEO.2021.120630.
84. Mansurbeg H, et al. Meteoric water incursion, crude oil degradation and calcite cementation of an upper cretaceous reservoir in the zagros foreland Basin (Kurdistan Region of Iraq). Water. 2023;15(10):1953. https://doi.org/10.3390/W15101953.
85. Ferry JG. Fundamentals of methanogenic pathways that are key to the biomethanation of complex biomass. Curr Opin Biotechnol. 2011;22(3):351–7. https://doi.org/10.1016/J.COPBIO.2011.04.011.
86. Vinson DS, Blair NE, Martini AM, Larter S, Orem WH, McIntosh JC. Microbial methane from in situ biodegradation of coal and shale: a review and reevaluation of hydrogen and carbon isotope signatures. Chem Geol. 2017;453:128–45. https://doi.org/10.1016/j.chemgeo.2017.01.027.
87. Tong C, She CX, Yang P, Jin YF, Huang JF. Weak correlation between methane production and abundance of methanogens across three Brackish Marsh Zones in the Min River Estuary, China. Estuaries Coasts. 2015;38(6):1872–84. https://doi.org/10.1007/S12237-014-9930-2/FIGURES/7.
88. Bräuer SL, Cadillo-Quiroz H, Ward RJ, Yavitt JB, Zinder SH. Methanoregula boonei gen. nov., sp. nov., an acidiphilic methanogen isolated from an acidic peat bog. Int J Syst Evol Microbiol. 2011;61(1):45–52. https://doi.org/10.1099/ijs.0.021782-0.
89. Yashiro Y, Sakai S, Ehara M, Miyazaki M, Yamaguchi T, Imachi H. *Methanoregula formicica* sp. nov., a methane-producing archaeon isolated from methanogenic sludge. Int J Syst Evol Microbiol. 2011;61(1):53–9. https://doi.org/10.1099/IJS.0.014811-0/CITE/REFWORKS.

90. Evans PN, et al. An evolving view of methane metabolism in the Archaea. Nat Rev Microbiol. 2019;17(4):219–32. https://doi.org/10.1038/s41579-018-0136-7.
91. Garcia PS, Gribaldo S, Borrel G. Diversity and evolution of methane-related pathways in Archaea. Annu Rev Microbiol. 2022;76:727–55. https://doi.org/10.1146/ANNUREV-MICRO-041020-024935/1.
92. Ferry JG, Smith PH, Wolfe RS. *Methanospirillum*, a new genus of methanogenic bacteria, and characterization of *methanospirillum hungatii* sp.nov. Int J Syst Bacteriol. 1974;24(4):465–9. https://doi.org/10.1099/00207713-24-4-465/CITE/REFWORKS.
93. Huser BA, Wuhrmann K, Zehnder AJB. *Methanothrix soehngenii* gen. nov. sp. nov., a new acetotrophic non-hydrogen-oxidizing methane bacterium. Arch Microbiol. 1982;132(1):1–9. https://doi.org/10.1007/BF00690808/METRICS.
94. Borrel G, et al. *Methanomethylophilus alvi* gen. nov., sp. nov., a novel hydrogenotrophic methyl-reducing methanogenic archaea of the order Methanomassiliicoccales isolated from the human gut and proposal of the novel family Methanomethylophilaceae fam. nov. Microorganisms. 2023;11(11):1. https://doi.org/10.3390/MICROORGANISMS11112794.
95. Leu AO, et al. Anaerobic methane oxidation coupled to manganese reduction by members of the Methanoperedenaceae. ISME J. 2020;14(4):1030–41. https://doi.org/10.1038/s41396-020-0590-x.
96. Martini AM, Walter LM, Ku TCW, Budai JM, McIntosh JC, Schoell M. Microbial production and modification of gases in sedimentary basins: A geochemical case study from a Devonian shale gas play, Michigan basin. Am Asso Petrol Geol Bull. 2003;87(8):1355–75. https://doi.org/10.1306/031903200184.
97. Mcintosh JC, Walter LM, Martini AM. Pleistocene recharge to midcontinent basins: Effects on salinity structure and microbial gas generation. 2002. https://doi.org/10.1038/383155a0.
98. Strapoć D, Mastalerz M, Schimmelmann A, Drobniak A, Hedges S. Variability of geochemical properties in a microbially dominated coalbed gas system from the eastern margin of the Illinois Basin, USA. Int J Coal Geol. 2008;76(1–2):98–110. https://doi.org/10.1016/j.coal.2008.02.002.
99. D. Strąpoć, et al. Methane-producing microbial community in a coal bed of the Illinois Basin. Appl Environ Microbiol. 2008;74(8):2424–32. https://doi.org/10.1128/AEM.02341-07.
100. Schlegel ME, McIntosh JC, Bates BL, Kirk MF, Martini AM. Comparison of fluid geochemistry and microbiology of multiple organic-rich reservoirs in the Illinois Basin, USA: Evidence for controls on methanogenesis and microbial transport. Geochim Cosmochim Acta. 2011;75(7):1903–19. https://doi.org/10.1016/j.gca.2011.01.016.
101. Waldron PJ, Petsch ST, Martini AM, Nüslein K. Salinity constraints on subsurface archaeal diversity and methanogenesis in sedimentary rock rich in organic matter. Appl Environ Microbiol. 2007;73(13):4171–9. https://doi.org/10.1128/AEM.02810-06.